AIAA JOURNAL
Vol. 41, No. 5, May 2003

Velocity Measurements in a Three-Dimensional Compressible Base Flow

Brad A. Boswell*
Sandia National Laboratories, Albuquerque, New Mexico 87185
and
J. Craig Dutton†
University of Illinois at Urbana–Champaign, Urbana, Illinois 61801

The velocity field in the base region of a circular cylinder with a length-to-radius ratio of 3.0 aligned at a 10-deg angle of attack to a nominal Mach 2.5 freestream has been investigated experimentally. The objective is to better understand the mechanisms that govern the characteristics and development of three-dimensional, compressible base flows. Laser Doppler velocimetry was used to measure both mean velocity components and turbulence statistics. The results reveal all expected base flow features, including a low-speed recirculation region, a separated shear layer, a reattachment region, and a trailing wake. The distance from the base to the rear stagnation point in this three-dimensional base flow is reduced by 55% as compared to the corresponding axisymmetric base flow. The shear layer in the leeward region of the flow turns sharply toward the radial centerline, resulting in a shift of the flow stagnation location toward the windward side of the base flow. In addition, the shear layer in the leeward plane thickens at a substantially faster rate than in either the windward or side planes. The turbulent stresses in the windward region of the shear layer are larger in magnitude than observed in either the leeward or side regions. The peak stresses measured in this three-dimensional base flow are located in the reattachment region, in direct contrast to axisymmetric results, where peak stresses were measured in the shear layer just upstream of reattachment.

Nomenclature

k	=	turbulent kinetic energy
L	=	projectile length
M	=	Mach number
P	=	turbulence production
R	=	base radius
r	=	radial coordinate
V	=	mean velocity
v	=	instantaneous velocity
x	=	axial coordinate
α	=	angle of attack
ϕ	=	circumferential coordinate
$\langle\ \rangle$	=	ensemble average

Subscripts

r	=	radial component
rev	=	reverse direction (upstream toward base surface)
stag	=	stagnation location
x	=	axial component
ϕ	=	circumferential component
∞	=	freestream condition

Superscript

$'$	=	fluctuation from the mean value

Presented as Paper 2002-0292 at the AIAA 40th Aerospace Sciences Meeting, Reno, NV, 14–17 January 2002; received 11 June 2002; revision received 18 October 2002; accepted for publication 6 January 2003.

*Senior Member of Technical Staff, Department 2132. Member AIAA.
†W. Grafton and Lillian B. Wilkins Professor, Department of Mechanical and Industrial Engineering. Associate Fellow AIAA.

Introduction

A COMPRESSIBLE base flow is generated in the near-wake region of various cylindrical slender bodies in supersonic flight, including missiles, rockets, and projectiles. The behavior of the flow in the base region is critical in determining the overall drag on the body. The flow structure in the base region of axisymmetric bodies in supersonic flight at zero angle of attack has been extensively investigated both experimentally and numerically throughout the past two decades.[1–8] Although the numerous flow features present in axisymmetric compressible base flows have presented substantial challenges in the efforts to understand the flow physics in the near-wake region, additional complexities are created when these aerodynamic bodies are inclined to nonzero angle of attack. Some of these additional factors include three dimensionality in the boundary layer prior to separation, the resulting circumferential flow in the boundary layer and in the base region and the potential for leeside separation vortex development. As a result of these additional complexities, only a few researchers have successfully obtained reliable experimental results in three-dimensional, compressible base flows.

To date, experimental efforts in three-dimensional compressible base flows have been restricted to measurements of base pressure to provide base-drag information for missile and projectile designers. Even these experimental efforts have been hindered by the sensitivity of base pressure to any support-interference effects present in the flow. In a review of compressible base-pressure data at angle of attack, Lamb and Oberkampf[9] found only two experimental studies that were free from support-interference effects.[10,11] Although both these studies provide excellent pressure measurements at the base surface, no detailed description of the base-flow structure is presented. Berner and Wey[12] were able to map the velocity field successfully in a three-dimensional base flow using three-component laser Doppler velocimetry (LDV), but results were obtained only for subsonic approach velocities, which do not recreate the wave structure present in supersonic base flows. To date, no detailed flowfield measurements have been completed to determine the fluid dynamic processes that control the behavior of a supersonic base flow at angle of attack.

This lack of detailed experimental flowfield data has hindered the efforts of researchers to validate computational models used

in predicting base-flow characteristics. Himeno et al.[13] computed a number of wake flowfields, including a three-dimensional base flow, but only for the case of a subsonic approach velocity. Using the three-dimensional thin-layer Navier–Stokes equations with the Baldwin–Lomax turbulence model, Sahu[14] extended his research on axisymmetric compressible base flows to investigate angle-of-attack effects in the transonic flow regime. However, no experimental results were available for comparison of the base-flow structure. Clearly, detailed experimental data in the base region of a cylindrical body inclined at nonzero angle of attack to a supersonic freestream are needed not only to understand the complex flow physics in this region, but also to provide a basis of comparison for improvement of future computational models of this flow. Interest in this investigation is by no means limited to the base-flow community alone, however, because this three-dimensional, turbulent, compressible flow provides a robust test case for the development and validation of turbulence models for use in compressible separated flows.

The current investigation seeks to provide detailed velocity data within the base region of a front sting-supported cylindrical afterbody inclined at 10-deg angle of attack to a Mach 2.45 freestream flow. Previously, this experimental facility has been used to visualize the base flowfield, measure the afterbody and base-surface pressure field, and measure the mean velocity and turbulence fields in the three-dimensional compressible boundary layer on the afterbody before separation.[15,16] The current investigation supplements this previous work with two-dimensional LDV measurements to determine both the mean-flow structure and turbulence statistics throughout the base region. A detailed analysis of these velocity results is performed to describe the flow physics that govern this complex, three-dimensional, separated flow interaction. In addition, the results are compared to the axisymmetric results of Herrin and Dutton[2,3,17] to determine the effects of three dimensionality on base-flow development.

Experimental Facilities and Procedures

The current experiments were conducted in a supersonic, blowdown-type wind tunnel designed specifically for the study of cylindrical base flows. For the current experimental conditions, with a stagnation pressure of 565 kPa and stagnation temperature of 300 K, the converging–diverging (C–D) nozzle of the facility provides an axisymmetric flow with a nominal freestream Mach number of 2.45 (at a unit Reynolds number of 56×10^6 m^{-1}) as the flow passes into the test section. The facility compressor system allows for a maximum tunnel run time of 45 s at steady-state operating conditions. Windows in the test section provide optical access to the near wake from three sides to allow for nonintrusive laser-diagnostic measurements and flow visualizations. To prevent flow interference from the nozzle boundary layer on the region of interest, pressure was monitored at the nozzle exit and in the test cell to verify that measurements were completed only when these pressures were matched. This pressure match results in infinitesimally weak waves that propagate from the nozzle exit, but do not impinge on the region of measurements. A complete description of the facility is included in Ref. 2.

A schematic of the angle-of-attack afterbody during run-on conditions is included in Fig. 1. The afterbody is connected via internal threads to a cylindrical sting that runs upstream along the tunnel centerline into the stagnation chamber, allowing for boundary-layer growth throughout the acceleration to supersonic speeds in the C–D nozzle. The sting is supported far upstream of the C–D nozzle to prevent interference effects from entering the measurement region. Oberkampf and Bartel[18] determined that forebody geometry does not significantly affect leeside vortex development along slender cylinders inclined at angle of attack in supersonic flow. As a result, the flowfield development along this cylindrical afterbody should be qualitatively similar to that present on a projectile in free flight. However, the geometry of a front sting support by no means accurately reflects the forebody of a supersonic projectile. Despite the minor effect of forebody geometry, the results presented subsequently cannot necessarily be expected to match results precisely that would be obtained for a projectile under identical free-flight conditions with a more realistic forebody geometry. However, the results do provide fundamental, interference-free insight into the mean flow and turbulence characteristics of a three-dimensional compressible base flow.

The cylindrical afterbody has a length-to-radius ratio of 3.0 and is inclined at a 10-deg angle of attack relative to the freestream flow. Previous investigations[15,16] revealed that no flow separation occurs in the leeward boundary layer of this afterbody. A cylindrical coordinate system is used throughout this investigation that is aligned along the normal to the base surface with positive axial x values oriented in the downstream direction. Radial distance r is measured from the base center. To prevent a discontinuity in the definition of the positive radial direction at the centerline for this three-dimensional flow, positive radial values are oriented in the leeward direction, and negative radial values are oriented in the windward direction, as shown in Fig. 1. Circumferential angle ϕ is measured from 0 deg on the windward surface to 180 deg on the leeward surface of the afterbody in a clockwise direction as observed from upstream.

A conventional two-component dual-beam LDV system was used in these experiments that was identical to that used in a previous investigation of the three-dimensional boundary layer on the afterbody surface.[16] Green (514.5-nm) and blue (488-nm) laser beams were generated by separating a 7-W argon-ion laser beam in a dispersion prism. The two beams were then split and converged to form a four-beam probe volume that was 165 μm in diameter, with fringe

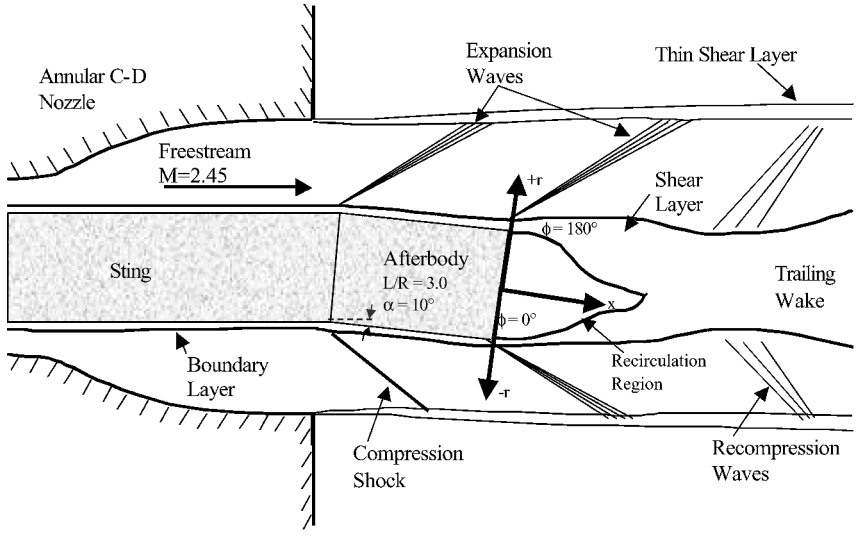

Fig. 1 Schematic of angle-of-attack afterbody and coordinate system.

spacings of 14.5 and 13.6 μm for the green and blue beams, respectively. Bragg cells were added to the optical system so that a 40-MHz frequency shift was generated in the downstream beam of each pair. This frequency shift is needed to reduce fringe biasing and discriminate reverse velocities in this highly three-dimensional flowfield. To reduce the possibility of fringe blindness, the beam pairs were also rotated to ± 45 deg from the incoming freestream flow direction. Once scattered by seed particles passing through the probe volume, the intensity of the laser light was collected at a 20-deg off-axis forward-scatter location, resulting in an effective probe-volume length of 730 μm. The light intensity was first converted to an analog voltage by two photomultiplier tubes. This voltage signal was then converted into the corresponding flow velocity using a TSI IFA-750 autocorrelation processor. The velocity data output from the IFA were collected using an Intel Celeron-based Personal Computer for postprocessing and analysis. The LDV probe volume was positioned through use of a three-axis, computer-controlled traverse system with a spatial resolution of ± 1.5 μm in all three directions.

The majority of the seeding for the LDV measurements was provided by a six-jet atomizer that supplied silicone oil droplets to the flow through three tubes located downstream of the flow conditioning section and separated by 120 deg circumferentially. However, a lack of freestream fluid mixing into the recirculation region resulted in an inadequate seed level and low data collection rates in the recirculation region. To increase the data rates in this region, additional silicone-droplet seeding was implemented via injection at extremely low flow rates through 17 separate 0.64-mm-diam holes (actually, pressure taps) on the base surface. One hole is located at the base center, and an additional four holes are separated by 6.35 mm each on the $\phi = -90$, 0, 90, and 180 deg radii. The velocity perturbations created by the injection jets were small and only observable very near the base in the low-turbulence recirculation region. From measurements performed immediately downstream of the seeding jets, the perturbations appear to persist less than approximately 8% of one base radius downstream of the base surface, which suggests that the injection influences only a small portion of the recirculation region in the flow. To further prevent the influence of the seed jets in the region of measurement, seeding holes in the plane of measurement were sealed during data acquisition. This base seeding provided an approximate injection parameter of $I = 5.73 \times 10^{-5}$, where I is the ratio of the injected mass flow rate to the freestream mass flux times the base area. This value is more than 250 times smaller than the injection parameter that resulted in peak base pressure for an axisymmetric base-bleed flow in a previous experiment in this facility.[19] In addition, the base injection resulted in only a 1% increase in base pressure, so that this injected seeding fluid has only a very minor influence on the base flowfield. The seeding system produces droplets with a mean diameter of 0.8 μm, which has been shown to be sufficiently small to follow the high-frequency turbulent fluctuations in this flow.[20]

For the current investigation, a series of radial profiles of mean velocity and turbulence statistics has been measured, with the measurements concentrated in the $\phi = 0/180$ and $-90/90$ deg planes, as seen in Fig. 2. In the $\phi = -90/90$-deg planes, additional measurements were extended 5 mm beyond the symmetry plane to verify optical alignment and the expected presence of the symmetry plane. Variations in mean velocity and velocity fluctuations remained consistently below 1% of the freestream velocity across the symmetry plane. Between 60 and 100 spatial locations are included in each radial traverse, with 4000 individual velocity realizations stored at each spatial location for the computation of turbulence statistics. Depending on the quantity of seed transported in the flow, sampling times at each spatial location varied from 1 s in the approach freestream to 35 s near the base in the recirculation region of the flow. An interarrival time weighting scheme has been used to treat the effects of velocity bias on the data. This method been shown to serve as an effective velocity debiasing tool in compressible shear flows.[21] With this two-component LDV optical arrangement, both the streamwise and radial components of the mean velocity can be measured simultaneously, but no measurements of the circumferential velocity component (which has a zero mean value in the $\phi = 0/180$ deg plane) can be obtained. For the current investigation, worst case mean velocity uncertainties are estimated as 1.73% V_∞ and 1.75% V_∞ for the axial and radial components, respectively. In addition, both axial and radial Reynolds normal stresses $\langle v_x'^2 \rangle$ and $\langle v_r'^2 \rangle$ and axial–radial Reynolds shear stress $\langle v_x' v_r' \rangle$ have been measured directly. Worst-case velocity fluctuation uncertainties are 2.02% V_∞ in the axial direction and 2.06% V_∞ for the radial component.

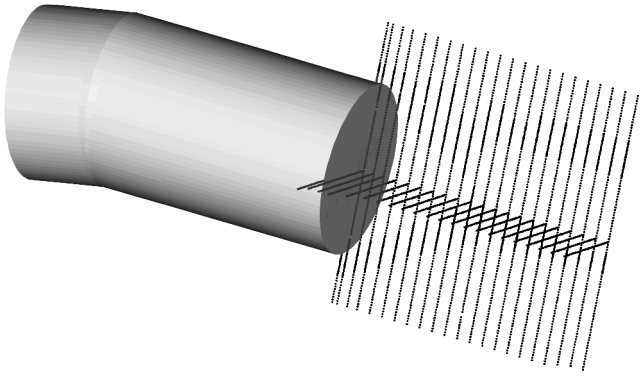

Fig. 2 LDV measurement locations in the current investigation.

Results and Discussion

Near-Wake Mean Velocity Measurements

The mean velocity vector field in the near-wake region of the three-dimensional base flow is included in Fig. 3, with Fig. 3a corresponding to the $\phi = 0/180$ deg symmetry side plane and Fig. 3b to the $\phi = -90/+90$ side planes. Note that, in the presentation of

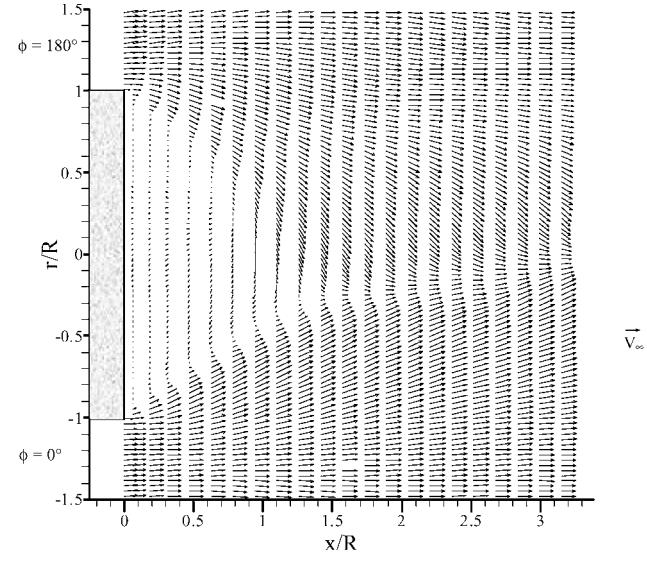

a) $\phi = 0/180$ deg plane

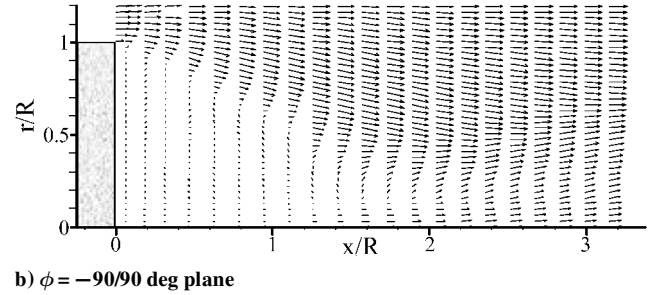

b) $\phi = -90/90$ deg plane

Fig. 3 Velocity vector field in near-wake region for a) $\phi = 0/180$ deg plane and b) $\phi = -90/90$ deg plane.

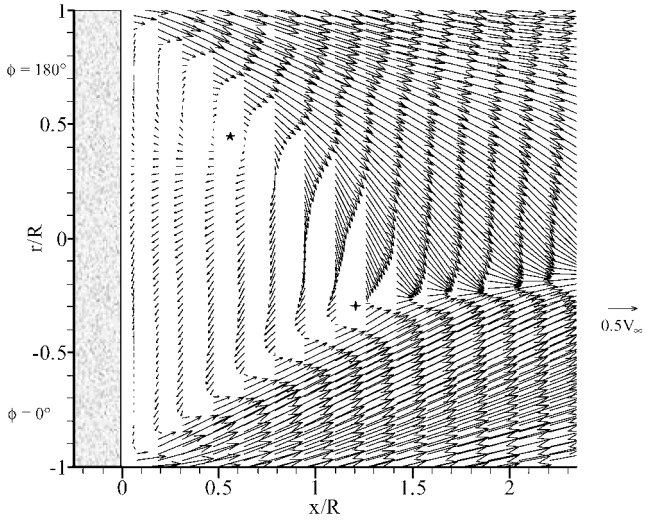

a) $\phi = 0/180$ deg plane

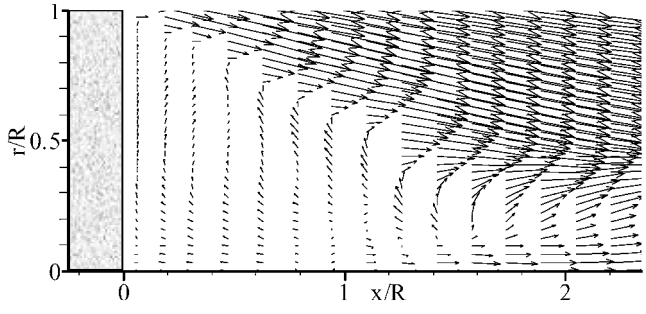

b) $\phi = -90/90$ deg plane

Fig. 4 Velocity vector field just downstream of base surface for a) $\phi = 0/180$ deg plane and b) $\phi = -90/90$ deg plane.

this vector field and as shown subsequently, the axial x scale has been compressed by a factor of 0.85 to better fit on the page. As seen in Fig. 2, the radial measurement spacing varies, with close spacing (as close as 0.25 mm) in regions of large gradients. To prevent the vector plot from becoming cluttered in regions of high measurement density, only vectors located radially at 1-mm intervals are presented in the Fig. 3 vector plots. All measurement locations are used in the generation of subsequent contour plots.

The Fig. 3 vector plot reveals the general flow structure expected in the base region. In both planes, the flow is observed to turn sharply just downstream of the base corner, where separation occurs. In the symmetry plane (Fig. 3a), the shear layer is turned more sharply in the leeward (top) region than in the windward region, resulting in a reattachment region at the convergence of the free shear layer that is shifted toward the windward from the radial base centerline. This shift is in contrast to the axisymmetric study of Herrin and Dutton,[2] where reattachment occurred directly on the axis of symmetry. This sharp turning of the shear layer in the leeward region was previously observed[15] as the entrainment of high-speed fluid into the recirculation region from the leeward portion of the flow in end-view Mie scattering flow visualizations. The entrainment of this leeward fluid into the recirculation region is also observed in the side plane (Fig. 3b) along the $r/R \approx 0$ line as larger magnitude velocity vectors begin to be observed at $x/R \approx 1.4$. The low-speed recirculation region is clearly observed just downstream of the base surface in both planes, with the recirculating fluid confined to an apparently much shorter axial length in the symmetry plane than in the side plane.

The features of the recirculation region can be more clearly observed in Fig. 4, which is a magnified view of the velocity vector field just downstream of the base surface. In Fig. 4, the vectors have been stretched to allow a clearer view of the behavior in the recirculation region. The structure of the recirculation region in the symmetry plane (Fig. 4a) differs significantly from the pair of symmetric recirculation lobes observed in the axisymmetric results.[2] First, the recirculation region occurs over a much shorter axial distance than in the previously observed axisymmetric study. Through linear interpolation of the symmetry plane velocity data, it is possible to approximate a location with both zero mean axial and radial velocity components that corresponds to a stagnation point because zero mean circumferential velocity is present in the symmetry plane. When this method is used, a stagnation point (four-point star in Fig. 4a) is observed at an axial distance of approximately $x/R \approx 1.2$ from the base. This stagnation distance is reduced by 55% from the axial stagnation length noted in the axisymmetric study of Herrin and Dutton,[2] where the stagnation location was measured to occur at $x/R = 2.65$ on the symmetry axis. Furthermore, the stagnation location appears to be displaced to a radial location of $r/R \approx -0.3$ on the windward side of the symmetry plane. The axial shift in the stagnation location is consistent with the low base pressure previously measured in this three-dimensional base flow, which is 48.4% below that of the axisymmetric case.[15] The radial shift in the stagnation point (and reattachment region) results from mean-flow three-dimensional effects and shear layer asymmetry.

The overall structure of the recirculation region appears as a reverse-s type of transport of fluid from leeward to windward. Fluid from the leeward side of the recirculation region is transported toward the base surface near $r/R \approx 0$. The fluid is then turned radially toward the windward portion of the flow, where it is entrained in the windward segment of the shear layer. In the leeward portion of the recirculation region, the flow appears to rotate about a point at $(x/R, r/R) \approx (0.55,\ 0.45)$ in this plane (five-point star in Fig. 4a). This rotation may be indicative of some type of circumferential vortex formation in the recirculation region. In the leeward region at $r/R \approx 0.3$, the flow appears to impinge directly on the base surface, a location corresponding closely to the location of a previously observed node of attachment.[15] In the windward portion of the recirculation region, an extremely low-speed region of flow occurs near the base surface at $r/R \approx -0.7$, near the location of a saddle point previously observed using base-surface flow visualization.[15] In the axisymmetric results of Herrin,[22] a node of attachment is present at the base centerline, but no saddle point is observed in the surface oil-streak visualization of the base surface.

The structure of the recirculation region in the side plane (Fig. 4b) is much different than that observed in the symmetry plane. Note that the velocity magnitude appears smaller in regions near the base, $x/R < 1.0$. This is most likely because no circumferential results have been measured, and thus, the side plane results are missing that important component in their magnitudes. However, note that low-speed fluid (at least for the components measured) persists much farther downstream in the side plane (in regions radially displaced from the $r = 0$ base centerline) than observed in the symmetry plane, which is indicative of the lobes of low-speed fluid previously observed using Mie scattering visualizations.[15]

Contours of the mean axial velocity in the near wake of the three-dimensional base flow are presented in Fig. 5. Note that the "wiggles" present (primarily in the separated shear layer just downstream of the base corner) in this (and subsequent) contour plots are nonphysical oscillations generated in the contouring process using these discretely spaced data. These nonphysical oscillations could be eliminated through collection of data with higher axial resolution. In the symmetry plane, the gradient of axial velocity, which is very large near the base corner separation point, appears to relax quickly in the leeward portion of the shear layer with increasing axial distance downstream. On the other hand, the gradient in the windward shear layer appears to maintain a larger magnitude with increased axial displacement from the base. Note that in the $\phi = 0/180$ deg symmetry plane, the remaining velocity defect at $x/R = 3.0$ occurs slightly on the leeward side of the centerline. In the recirculation region, a maximum reverse velocity of $V_x/V_\infty = -0.188$ was measured in the windward portion of the recirculation region at $(x/R, r/R) = (0.95, -0.35)$, as denoted by the star in Fig. 5a, an axial position 78% of the distance from the base to the stagnation location. In the axisymmetric base flow, by comparison, Herrin and

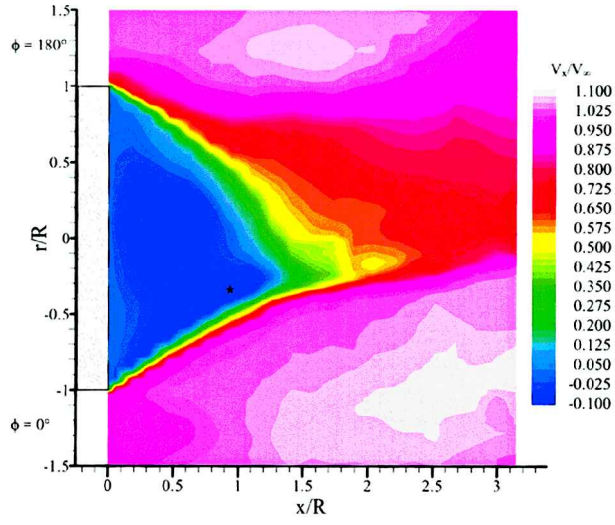

a) $\phi = 0/180$ deg plane

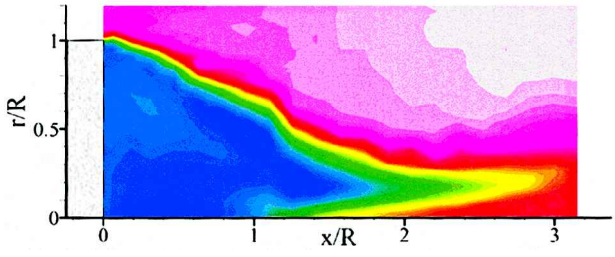

b) $\phi = -90/90$ deg plane

Fig. 5 Mean axial velocity contours in the near-wake region for a) $\phi = 0/180$ deg plane and b) $\phi = -90/90$ deg plane.

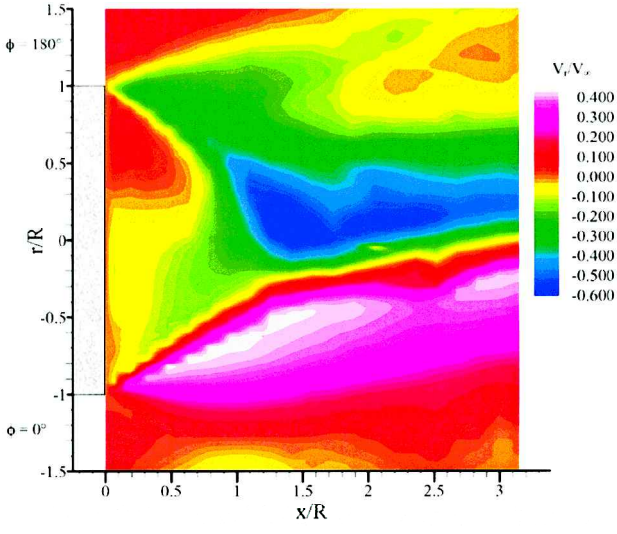

a) $\phi = 0/180$ deg plane

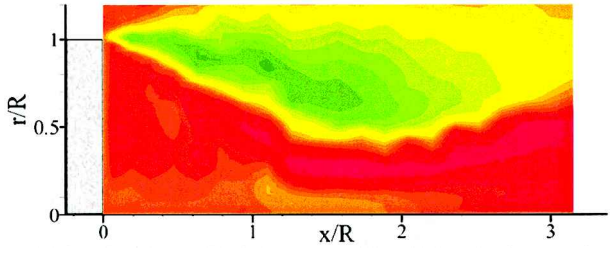

b) $\phi = -90/90$ deg plane

Fig. 6 Mean radial velocity contours in the near-wake region for a) $\phi = 0/180$ deg plane and b) $\phi = -90/90$ deg plane.

Dutton[2] measured a maximum reverse velocity of $V_x/V_\infty \approx -0.3$ on the axis of symmetry at an axial location of 64% of the distance to the stagnation point. The decrease in maximum reverse velocity for the three-dimensional case results from the short recirculation length, which provides a very short region for acceleration of the recirculating fluid toward the base. In the side plane, the entrainment of high axial velocity fluid on the $r = 0$ centerline results in an earlier axial acceleration of the fluid near $r = 0$ than observed for fluid displaced radially from the centerline.

Contours of the mean radial velocity in the near-wake region are included in Fig. 6. As mentioned earlier, a negative radial velocity in Fig. 6 refers to a velocity component from leeward to windward and normal to the radial centerline. In the symmetry plane, a sharp radial gradient in radial velocity occurs throughout the reattachment region. This gradient occurs because fluid in the windward shear layer maintains a positive radial velocity, and in the leeward shear layer, fluid possesses a negative radial velocity approaching reattachment. The location of zero radial velocity shifts from windward to leeward throughout the axial development of the reattachment region. In the side plane, significant radial velocity is confined primarily just outside the shear layer downstream of base separation, where the flow is turned toward the radial centerline (hence, the region of negative radial velocity in the shear layer). Note, however, that this region of negative radial velocity in the side plane is confined to the outer region of the flow ($r/R > 0.5$) because the flow in the recirculation region maintains quite small (and generally positive) radial velocity.

Two-dimensional Mach number contours for the near-wake region are included in Fig. 7. The shear layer in the leeward region clearly grows at a much faster rate, as determined from the divergence of the contours, than observed in the windward region. In the leeward region, a clear "dip" in the shear layer occurs just before reattachment because the fluid in the leeward shear layer is turned sharply toward the stagnation location. Also note again that the location of the velocity defect in the near wake appears to shift from windward to leeward throughout its postreattachment axial development.

The maximum Mach number in the symmetry plane (star in Fig. 7a) is $M = 3.31$ and is found at $(x/R, r/R) \approx (2.52, -0.60)$ in the windward region. This Mach number is 17% higher than the maximum measured Mach number in the axisymmetric study of Herrin and Dutton,[2] where the maximum Mach number of $M = 2.83$ was found at $(x/R,\ r/R) \approx (1.0, 1.0)$. Note that, in the axisymmetric study, the maximum Mach number was measured just downstream of the base-edge separation fan. In the three-dimensional case, this maximum Mach number occurs substantially downstream of the reattachment point, suggesting a very different type of reattachment process in this three-dimensional case. It appears that, downstream of reattachment, fluid located on the windward side of the wake is turned slightly toward the leeward as the velocity deficit in the wake translates from windward to leeward. This slight rotation of the windward fluid toward the leeward portion of the flow may act as a small expansion turn, accelerating the fluid in the windward region to the maximum measured Mach number. Thus, it appears that the "recompression" process in this three-dimensional flow is actually a combined recompression/reexpansion process, with strength varying circumferentially from windward to leeward.

In the side plane, the persistence of the lower speed recirculating fluid (at least in the $V_x - V_r$ sense) is again clearly evident just off the radial centerline of the plane, as previously observed in the flow visualizations.[15] In Fig. 7, note that the Mach number plotted includes only the $V_x - V_r$ velocity components and not the circumferential component, which was not measured.

Near-Wake Turbulence Measurements

Contours of turbulent axial normal stress, $\langle v_x'^2 \rangle / V_\infty^2$, in the near-wake region are included in Fig. 8. Relatively low axial normal stress fluid is present in the outer flow and recirculation region, with the high axial stress fluid confined to the shear layer and developing wake. Note that the axial stress in the windward portion of the shear layer is much stronger than that present in the leeward shear layer. Also, note a small increase in axial stress in the leeward

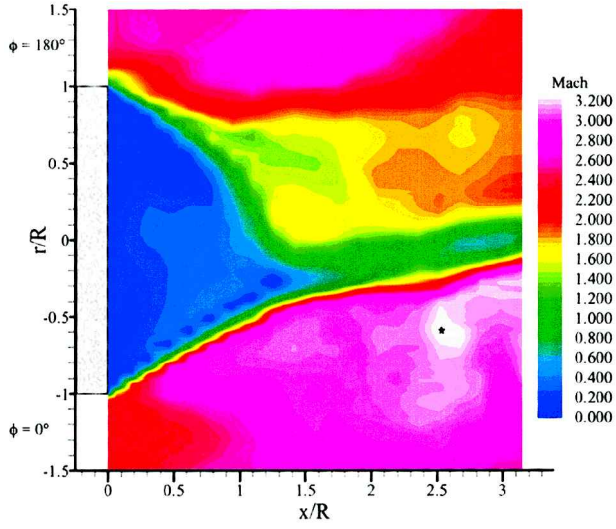

a) $\phi = 0/180$ deg plane

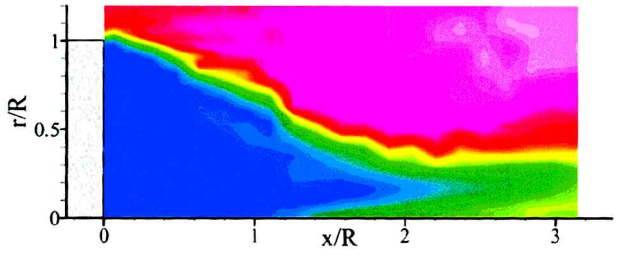

b) $\phi = -90/90$ deg plane

Fig. 7 Mean two-dimensional Mach number contours in the near-wake region for a) $\phi = 0/180$ deg plane and b) $\phi = -90/90$ deg plane.

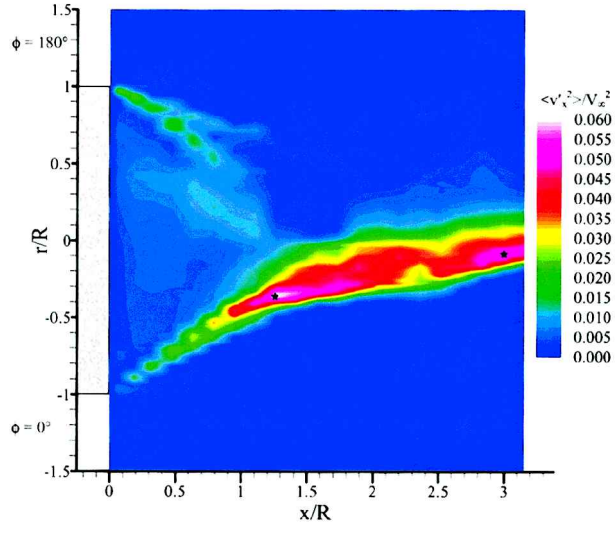

a) $\phi = 0/180$ deg plane

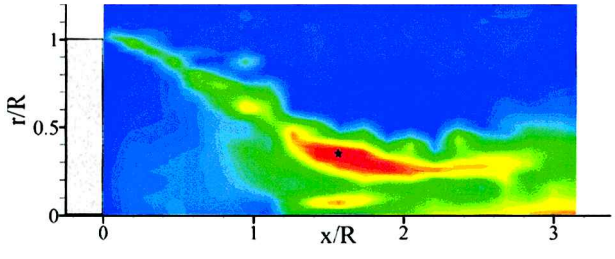

b) $\phi = -90/90$ deg plane

Fig. 8 Axial normal stress contours in the near-wake region for a) $\phi = 0/180$ deg plane and b) $\phi = -90/90$ deg plane.

portion of the recirculation region near the base surface at $r/R \approx 0.3$, where a node of attachment was observed in previous base-surface flow visualizations.[15] Two stress peaks are noted in the developing wake on the symmetry plane and are marked by stars in Fig. 8a. First, a peak axial stress of $\langle v_x'^2 \rangle / V_\infty^2 = 0.062$ was measured at $(x/R, r/R) = (1.26, -0.37)$ in the windward region, very near the location of the rear stagnation point and the onset of flow reattachment. A second peak in axial normal stress with $\langle v_x'^2 \rangle / V_\infty^2 = 0.061$ was measured at $(x/R, r/R) = (2.99, -0.09)$ in the windward portion of the developing wake. These axial stress peaks are larger than measured in the axisymmetric study of Herrin and Dutton,[2] where a peak axial stress of $\langle v_x'^2 \rangle / V_\infty^2 = 0.048$ was measured near the inner edge of the shear layer 83% of the axial distance from the base to the reattachment location. Furthermore, Herrin and Dutton[17] found a sharp decrease in axial stress through the reattachment region to levels in the developing wake that were lower than those observed in most of the shear layer. In this three-dimensional base flow, however, the axial stress in the developing wake remains significantly higher than observed in the shear layer. This shift of the peak axial stress to near and downstream of the reattachment point agrees with the results of Hayakawa et al.[23] and Samimy et al.[24] for the reattachment of a planar supersonic shear layer on a solid wall, that is, backstep flow. This agreement with a solid-wall reattachment is most likely fortuitous, though, because the mechanisms amplifying the axial turbulence in the reattachment region of the current flow are quite dissimilar. Instead, the reduced length of the shear layer in this three-dimensional base flow compared to the axisymmetric base flow (as evidenced by the short recirculation length) may result in increased axial dilatation of the fluid elements as they are compressed through the reattachment region. Hayakawa et al.[23] suggest that an increase in axial dilatation at reattachment increases the axial turbulence length scale, thus effectively increasing the axial normal stress.

In the side plane (Fig. 8b), the axial stress remains low in the recirculation region and outer flow. The axial stress in the side plane shear layer is similar in magnitude to that observed in the windward shear layer and is significantly higher than the normal stress in the leeward shear layer. A peak in the axial normal stress in the side plane was measured at $(x/R, r/R) = (1.58, 0.36)$, near the reattachment region, where $\langle v_x'^2 \rangle / V_\infty^2 = 0.043$. Also note that the region of higher axial normal stress diffuses radially in the recompression region and trailing wake from the radial centerline to a distance of $r/R \approx 0.5$.

Contours of radial normal stress, $\langle v_r'^2 \rangle / V_\infty^2$, are included in Fig. 9 for the symmetry and side planes. As in the axial normal stress results, high radial stress fluid is confined to the separated shear layer and trailing wake region. Note that the disparity in radial normal stress magnitude between the windward and leeward regions of the shear layer is even greater than that observed for the axial normal stress. Radial normal stress magnitudes in the windward shear layer are approximately three times greater than those observed in the leeward shear layer. The peak radial normal stress in the symmetry plane was measured at $(x/R, r/R) = (2.21, -0.06)$ downstream of the reattachment point, where $\langle v_r'^2 \rangle / V_\infty^2 = 0.084$, a value 35% higher than the measured axial normal stress peak in the trailing wake. This radial normal stress is significantly higher (over three times) than the maximum value of Herrin and Dutton,[2] who measured a peak radial normal stress of $\langle v_r'^2 \rangle / V_\infty^2 = 0.024$ upstream of the reattachment point for the axisymmetric case. Downstream of the reattachment point, the radial turbulent stress magnitude diminishes greatly in magnitude in the axisymmetric results, which is not the case for the three-dimensional base flow shown in Fig. 9. The three dimensionality of the reattachment process in the current study results in a significant increase of radial momentum in the rapidly converging shear layer, which results in amplification of the turbulent radial normal stress.

In the side plane (Fig. 9b), the radial normal stress in the shear layer downstream of the base surface is quite low in magnitude ($\langle v_r'^2 \rangle / V_\infty^2 < 0.015$), levels closer in magnitude to those observed in the leeward shear layer (maximum $\langle v_r'^2 \rangle / V_\infty^2 \approx 0.011$) than the windward shear layer (maximum $\langle v_r'^2 \rangle / V_\infty^2 \approx 0.026$). Note that this trend is reversed from that observed from the axial stress contours, where the side shear layer stress level more closely resembles the

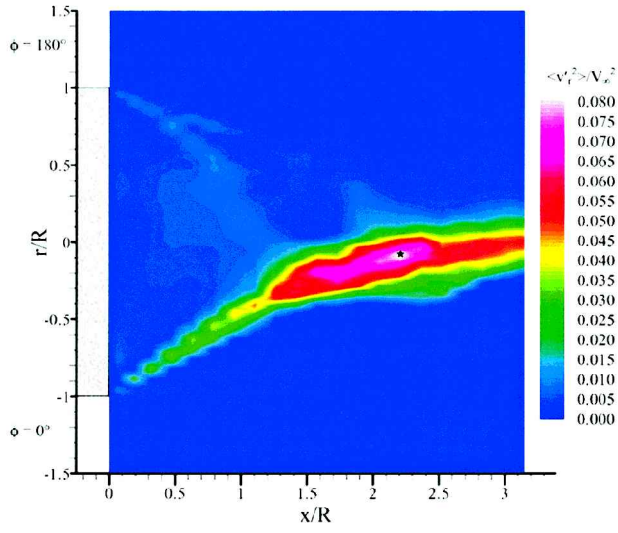

a) $\phi = 0/180$ deg plane

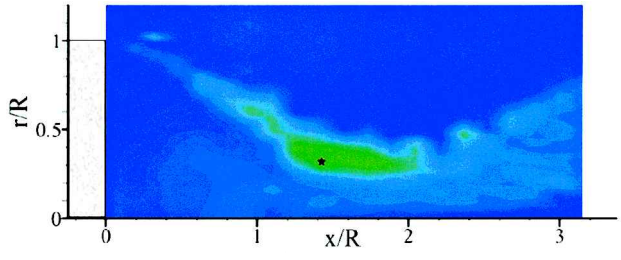

b) $\phi = -90/90$ deg plane

Fig. 9 Radial normal stress contours in the near-wake region for a) $\phi = 0/180$ deg plane and b) $\phi = -90/90$ deg plane.

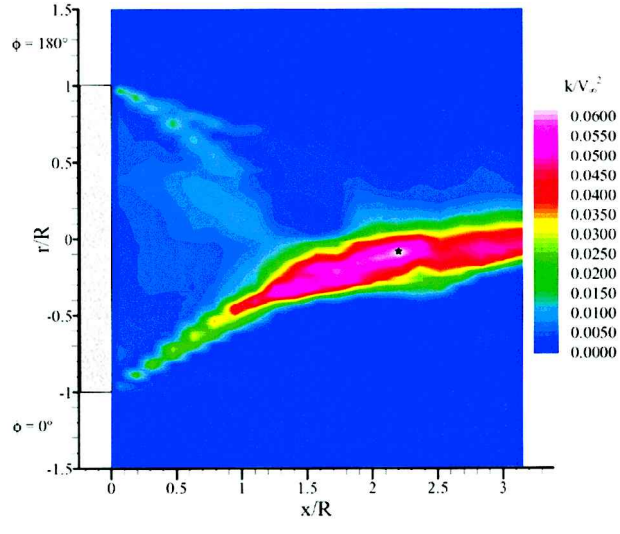

a) $\phi = 0/180$ deg plane

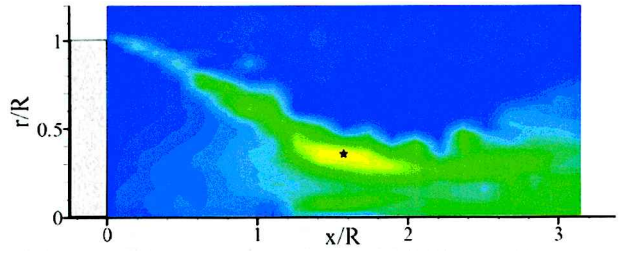

b) $\phi = -90/90$ deg plane

Fig. 10 Contours of axial–radial turbulent kinetic energy in the near-wake region for a) $\phi = 0/180$ deg plane and b) $\phi = -90/90$ deg plane.

windward shear layer. Just downstream of the reattachment location, a side plane peak in radial normal stress is measured at $(x/R, r/R) = (1.42, 0.32)$, where $\langle v_r'^2 \rangle / V_\infty^2 = 0.026$. Note that this amplification of radial stress is much smaller than observed in the symmetry plane ($\langle v_r'^2 \rangle / V_\infty^2 = 0.084$), which suggests that the radial momentum increase is reduced in this side plane where shear layer convergence is not as severe at reattachment as observed in the symmetry plane.

Figure 10 provides contours of the nondimensional turbulent kinetic energy k/V_∞^2 in the near-wake region. Using the following two-dimensional definition of turbulent kinetic energy:

$$k = \tfrac{1}{2}\left(\langle v_x'^2 \rangle + \langle v_r'^2 \rangle\right) \tag{1}$$

where k has been calculated using only the two directly measured normal stresses. Note that the circumferential normal stress is not included in the calculation of k because this stress was not measured, and the high variation of anisotropy in this three-dimensional flow makes the estimation of this stress highly uncertain. Qualitatively, the contours of turbulent kinetic energy appear to match the contours of whichever normal stress is larger at the point of interest. In the shear layer, higher k is observed in the windward and side regions than in the leeward region due to the very small radial stress present in the leeward portion of the shear layer. In the side plane, the diffusion of high axial stress fluid across the trailing wake results in a broad region of fluid with moderately high turbulent kinetic energy. In the $\phi = 0/180$-deg symmetry plane, the peak measurement of turbulent kinetic energy [$k/V_\infty^2 = 0.064$ at $(x/R, r/R) = (2.21, -0.09)$ in the windward region] nearly matches the location of measured maximum radial normal stress. However, note that the sum of the normal stresses results in a broader region of high k in the trailing wake due to a slight windward displacement of the high radial stress fluid compared to the high axial stress fluid far downstream. This measured peak in turbulent kinetic energy is significantly higher than the measured peak of Herrin and Dutton[2] in an axisymmetric base flow ($k/V_\infty^2 = 0.044$ in the shear layer before reattachment), despite that all three normal stresses were included in the calculation of the axisymmetric result. The three dimensionality generated by the inclination to nonzero angle of attack thus produces substantially higher turbulent kinetic energy than for a base flow at zero angle of attack.

Contours of axial–radial Reynolds shear stress ($-\langle v_x' v_r' \rangle / V_\infty^2$) in the near-wake region are included in Fig. 11 for the symmetry and side planes. As observed in the normal stress results, no significant shear stress is measured in the recirculation region, which is indicative of a lack of large-scale turbulent structure in this region. In addition, the shear stress magnitude remains significantly higher on the windward side of the shear layer than in the leeward or side regions upstream of the reattachment point. In the developing wake downstream of the reattachment point in the symmetry plane, a small region of shear stress of the opposite sign is observed near the radial centerline. This sign change occurs in the trailing wake at radial locations approximately corresponding to the position of zero mean radial velocity, which suggests that the region of flow realignment that occurs in the trailing wake results in a reversal of the shear stress acting on fluid elements in this region. Two peaks in shear stress are noted in the symmetry plane. The first peak is measured near the reattachment point at $(x/R, r/R) = (1.26, -0.36)$ in the windward region, where $-\langle v_x' v_r' \rangle / V_\infty^2 = 0.039$. The second peak in shear stress is measured far downstream of the reattachment point in the trailing wake at $(x/R, r/R) = (2.99, -0.13)$, a location in the flow where $-\langle v_x' v_r' \rangle / V_\infty^2 = 0.044$. Note that both of these peaks are significantly larger than the maximum axial–radial shear stress measured by Herrin and Dutton[2] for an axisymmetric base flow, where a peak of $-\langle v_x' v_r' \rangle / V_\infty^2 = 0.019$ was measured upstream of the reattachment location. This shear stress magnitude observed in the axisymmetric base flow is similar in magnitude to the shear stresses observed in the windward region of the shear layer before reattachment for the current case.

In the side plane (Fig. 11b), a sign change in the shear stress is observed between the side shear layer and the radial centerline near

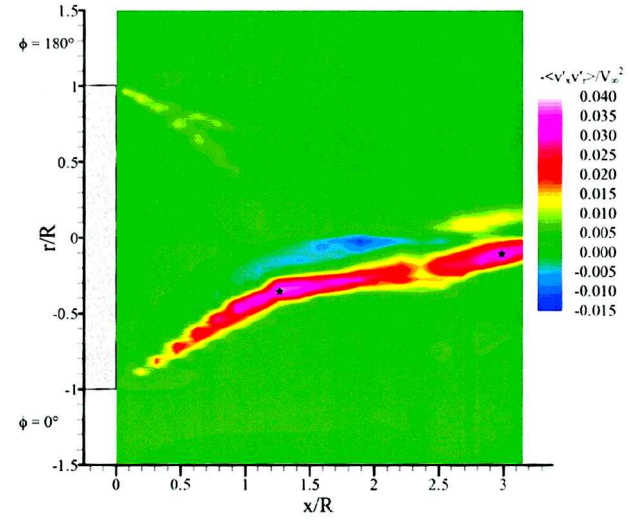

a) $\phi = 0/180$ deg plane

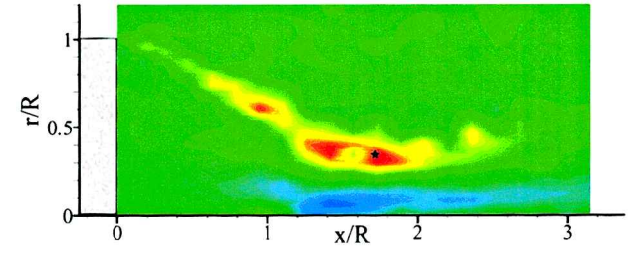

b) $\phi = -90/90$ deg plane

Fig. 11 Axial–radial Reynolds shear stress contours in the near-wake region for a) $\phi = 0/180$ deg plane and b) $\phi = -90/90$ deg plane.

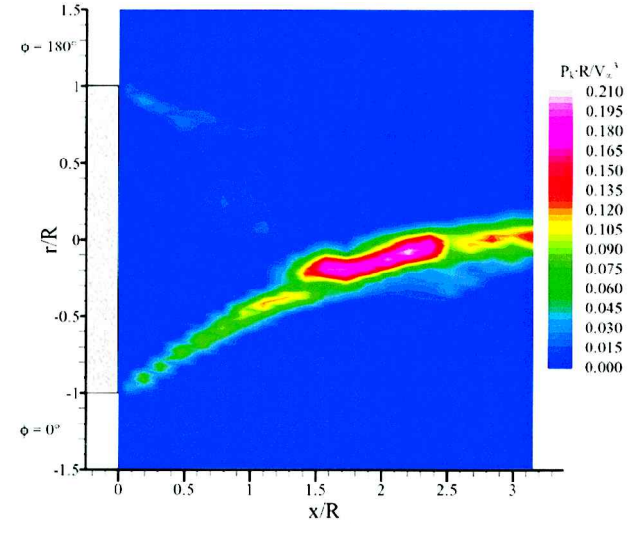

a) $\phi = 0/180$ deg plane

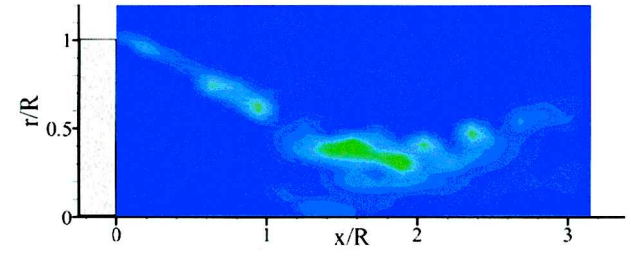

b) $\phi = -90/90$ deg plane

Fig. 12 Turbulent kinetic energy production contours in the near-wake region for a) $\phi = 0/180$ deg plane and b) $\phi = -90/90$ deg plane.

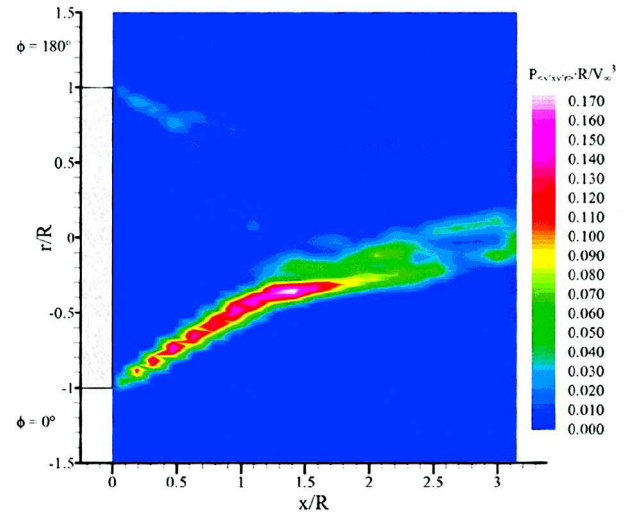

a) $\phi = 0/180$ deg plane

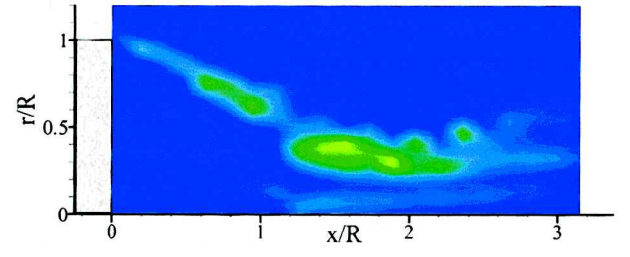

b) $\phi = -90/90$ deg plane

Fig. 13 Axial–radial shear stress production contours in the near-wake region for a) $\phi = 0/180$ deg plane and b) $\phi = -90/90$ deg plane.

the reattachment location. This region of oppositely signed shear stress occurs in the region of strong leeward to windward secondary flow previously observed in Mie scattering flow visualizations (see Ref. 15), that is, in a region of strong circumferential flow normal to the plane of Fig. 11b. The change in sign of shear stress between these regions may be indicative of a change in the favored orientation of large-scale turbulent structures in the outer shear layer and the inner entrained fluid region. The low shear stress region between the positive and negative shear stress areas corresponds to the low-speed $(V_x - V_r)$ recirculating fluid that persists farther downstream in this side plane than in the symmetry plane. This low-speed region is devoid of large-scale structures in the flow visualizations, thus, leading to the low shear stress measurements.

The generation of turbulent kinetic energy can be quantified through analysis of the turbulence production P_k, which describes the transfer of energy from the mean flow into the turbulent kinetic energy. The turbulence production is defined as

$$P_k = -\langle v_i' v_j' \rangle \frac{\partial V_i}{\partial x_j} \tag{2}$$

where repetition of the subscripts i and j denote summation of all three components and x is one of the three coordinate directions. Because only three of the six turbulent stresses have been measured directly, the turbulence production calculated in the current investigation reduces to the following form:

$$P_k = -\langle v_x'^2 \rangle \frac{\partial V_x}{\partial x} - \langle v_r'^2 \rangle \frac{\partial V_r}{\partial r} - \langle v_x' v_r' \rangle \left(\frac{\partial V_x}{\partial r} + \frac{\partial V_r}{\partial x} \right) \tag{3}$$

A contour map of turbulent kinetic energy production in the near wake (nondimensionalized by the base radius and freestream velocity cubed) for both the symmetry and side planes is included in Fig. 12. Results in the symmetry plane reveal a region of very high-turbulence production in the developing wake just downstream of the

reattachment location. The peak production of turbulent kinetic energy, $P_k R/V_\infty^3 = 0.24$, is significantly larger than the peak axisymmetric production of Herrin and Dutton,[2] where $P_k R/V_\infty^3 = 0.13$ was measured directly downstream of the base-edge separation point for the axisymmetric geometry. Note that turbulence production levels in the majority of the free shear layer regions of the current study are much smaller in all three measurement planes than in the axisymmetric case. This trend suggests that the stabilizing effects of the expansion at separation have been increased by flow three dimensionality. Furthermore, note that turbulence production in the side plane is significantly lower than in the windward region and trailing wake of the symmetry plane, with a modest increase in production near the reattachment location in the outer shear layer.

Based on the Reynolds stress transport equation, the production of axial–radial shear stress is defined in the following equation:

$$P_{\langle v_x' v_r' \rangle} = \langle v_x'^2 \rangle \frac{\partial V_r}{\partial x} + \langle v_r'^2 \rangle \frac{\partial V_x}{\partial r} + \langle v_x' v_r' \rangle \left(\frac{\partial V_x}{\partial x} + \frac{\partial V_r}{\partial r} \right) \qquad (4)$$

Note that, in this form, a positive value of shear stress production represents an increase in shear stress magnitude, although the shear stress actually becomes more negative. Contours of dimensionless shear stress production in the near-wake region are included in Fig. 13. The highest shear-stress production is observed in the windward shear layer, with a peak in production of $P_{\langle v_x' v_r' \rangle} \cdot R/V_\infty^3 = 0.235$ just downstream of the reattachment location, near $x/R \approx 1.3$. This is in contrast to the production of turbulent kinetic energy, for which the maximum is located in the developing wake downstream of the reattachment location, as shown in Fig. 12. This high shear stress production results from the high radial velocity gradients [the last partial derivative in Eq. (4)] that occur as part of the flow realignment process in this high shear stress region. This location of peak shear-stress production also contrasts with the results of Herrin,[22] for which a maximum shear stress production of $P_{\langle v_x' v_r' \rangle} \cdot R/V_\infty^3 = 0.20$ was found in the inner portion of the shear layer just downstream of the base-edge separation. Herrin then noted a rapid decrease in production with axial displacement from the base surface. The lack of high shear stress production in the reattachment region in the axisymmetric case most likely results from the combination of reduced shear stresses in this region and a smaller radial velocity gradient because the flow realignment is less severe in the axisymmetric flow, especially compared to the leeward region of the three-dimensional shear layer. Finally, note that shear stress production is much smaller in magnitude in the side region than in the windward region of the shear layer.

Conclusions

LDV has been used to measure the mean velocity and turbulence fields in a three-dimensional compressible base flow. This base flow was generated by inclining a 63.5-mm-diam cylindrical afterbody to 10-deg angle of attack in a Mach 2.45 freestream. This study permits determination of the physical behavior of this three-dimensional base flow and provides understanding of the fluid dynamic processes that occur downstream of cylindrical afterbodies when rotated from zero to nonzero angle of attack. Based on the velocity measurements, the following conclusions may be drawn:

1) The reduced base pressure in this three-dimensional separated flow results in a much shorter recirculation region (stagnation length reduced by 55%) than observed in the axisymmetric case.[2] In addition, the stagnation location is shifted toward the windward side of the base flow, resulting from a more severe angle of convergence in the leeward region of the shear layer than observed in the windward plane. In the recirculation region, the reverse flow is generally oriented from leeward to windward before entrainment in the windward shear layer. In the side plane, the presence of low-speed fluid remnants, slightly displaced from the radial centerline, which were originally observed in Mie scattering visualizations (see Ref. 15), are confirmed in the velocity measurements.

2) The shear layer appears to grow at a faster rate in the leeward region of the flow than in the windward region. As the shear layer develops, though, the inner edge of the leeward shear layer turns sharply toward the radial centerline, resulting in a substantial increase in the leeward shear-layer growth rate. In the side plane, the shear layer converges at a shallower angle than observed in either the windward or leeward planes.

3) Peak levels of turbulent stress in the base region are generally confined to the shear layer and trailing wake. The maximum levels of turbulent stress are located just downstream of reattachment on the windward side of the trailing wake. This peak stress location contrasts with the axisymmetric case,[2] where the maximum stress was measured near the inner edge of the shear layer just before flow reattachment. In general, the axial and radial normal stresses are similar in magnitude, and both of these stresses are larger than the measured axial–radial shear stress. In addition, all three stresses tend to be larger in the windward shear layer than noted in either the side or leeward shear layers.

4) Turbulent kinetic energy production in the three-dimensional base flow is significantly greater than measured in the axisymmetric case.[2] Peaks in turbulent kinetic energy production are located just downstream of the reattachment location. The maximum shear stress production is observed in the windward shear layer as a result of the large radial velocity gradient present in the windward shear layer. In the side plane, both the turbulent kinetic energy and shear stress production levels are much lower than observed in the symmetry plane.

Acknowledgments

This work was supported by the U.S. Army Research Office, under Grant DAAD19-01-1-0367, with Thomas L. Doligalski as Technical Monitor. Electronic copies of these data are available for use in model development and validation. To obtain a copy, contact either B. Boswell at baboswe@sandia.gov or C. Dutton at j-dutton@uiuc.edu.

References

[1]Gaviglio, J., Dussauge, J.-P., Debieve, J.-F., and Favre, A., "Behavior of a Turbulent Flow, Strongly Out of Equilibrium, at Supersonic Speeds," *Physics of Fluids*, Vol. 20, No. 10, Pt. II, 1977, pp. 179–192.

[2]Herrin, J. L., and Dutton, J. C., "Supersonic Base Flow Experiments in the Near Wake of a Cylindrical Afterbody," *AIAA Journal*, Vol. 32, No. 1, 1994, pp. 77–83.

[3]Herrin, J. L., and Dutton, J. C., "Effect of a Rapid Expansion on the Development of Compressible Free Shear Layers," *Physics of Fluids*, Vol. 7, No. 1, 1995, pp. 159–171.

[4]Bourdon, C. J., and Dutton, J. C., "Planar Visualizations of Large-Scale Turbulent Structures in Axisymmetric Supersonic Separated Flows," *Physics of Fluids*, Vol. 11, No. 1, 1999, pp. 201–213.

[5]Sahu, J., "Numerical Computations of Supersonic Base Flow with Special Emphasis on Turbulence Modeling," *AIAA Journal*, Vol. 32, No. 7, 1994, pp. 1547–1549.

[6]Tucker, P. K., and Shyy, W., "A Numerical Analysis of Supersonic Flow over an Axisymmetric Afterbody," AIAA Paper 93-2347, June 1993.

[7]Chuang, C.-C., and Chieng, C.-C., "Supersonic Base-Flow Computation Using Higher-Order Closure Turbulence Models," *Journal of Spacecraft and Rockets*, Vol. 33, No. 3, 1996, pp. 374–380.

[8]Fureby, C., Nilsson, Y., and Andersson, K., "Large Eddy Simulation of Supersonic Base Flow," AIAA Paper 99-0426, Jan. 1999.

[9]Lamb, J. P., and Oberkampf, W. L., "Review and Development of Base Pressure and Base Heating Correlations in Supersonic Flow," *Journal of Spacecraft and Rockets*, Vol. 32, No. 1, 1995, pp. 8–23.

[10]Pick, G. S., "Base Pressure Distribution of a Cone at Hypersonic Speeds," *AIAA Journal*, Vol. 10, No. 12, 1972, pp. 1685–1686.

[11]Moore, F. G., Hymer, T., and Wilcox, F. J., "Improved Empirical Model for Base Drag Prediction on Missile Configurations Based on New Wind Tunnel Data," U.S. Naval Surface Warfare Center, NSWCDD/TR-92/509, 1992.

[12]Berner, C., and Wey, P., "Measurements, Visualization and Interpretation of 3-D Flows Application within Base Flows," *IEEE Aerospace and Electronic Systems Magazine*, Vol. 5, No. 2, 1990, pp. 10–18.

[13]Himeno, R., Shirayama, S., Kamo, K., and Kuwahara, K., "Computational Study of Three-Dimensional Wake Structure," AIAA Paper 85-1617, July 1985.

[14]Sahu, J., "Three-Dimensional Base Flow Calculation for a Projectile at Transonic Velocity," AIAA Paper 86-1051, May 1986.

[15]Boswell, B. A., and Dutton, J. C., "Flow Visualizations and Measurements of a Three-Dimensional Supersonic Separated Flow," *AIAA Journal*, Vol. 39, No. 1, 2001, pp. 113–121.

[16]Boswell, B. A., and Dutton, J. C., "Velocity Measurements in a Pressure-Driven Three-Dimensional Compressible Turbulent Boundary Layer," *AIAA Journal*, Vol. 40, No. 7, 2002, pp. 1300–1310.

[17]Herrin, J. L., and Dutton, J. C., "The Turbulence Structure of a Reattaching Axisymmetric Compressible Free Shear Layer," *Physics of Fluids*, Vol. 9, No. 11, 1997, pp. 3502–3512.

[18]Oberkampf, W. L., and Bartel, T. J., "Symmetric Body Vortex Wake Characteristics in Supersonic Flow," *AIAA Journal*, Vol. 18, No. 11, 1980, pp. 1289–1297.

[19]Mathur, T., and Dutton, J. C., "Base-Bleed Experiments with a Cylindrical Afterbody in Supersonic Flow," *Journal of Spacecraft and Rockets*, Vol. 33, No. 1, 1996, pp. 30–37.

[20]Bloomberg, J. E., "An Investigation of Particle Dynamics Effects Related to LDV Measurements in Compressible Flows," M.S. Thesis, Dept. of Mechanical and Industrial Engineering, Univ. of Illinois, Urbana, IL, May 1989.

[21]Herrin, J. L., and Dutton, J. C., "An Investigation of LDV Velocity Bias Correction Techniques for High Speed Separated Flows," *Experiments in Fluids*, Vol. 14, 1993, pp. 354–363.

[22]Herrin, J. L., "An Experimental Investigation of Supersonic Axisymmetric Base Flows Including the Effects of Afterbody Boattailing," Ph.D. Dissertation, Dept. of Mechanical and Industrial Engineering, Univ. of Illinois, Urbana, IL, July 1993.

[23]Hayakawa, K., Smits, A. J., and Bogdonoff, S. M., "Turbulence Measurements in a Compressible Reattaching Shear Layer," *AIAA Journal*, Vol. 22, No. 7, 1984, pp. 889–895.

[24]Samimy, M., Petrie, H. L., and Addy, A. L., "A Study of Compressible Turbulent Reattaching Free Shear Layers," *AIAA Journal*, Vol. 24, No. 2, 1986, pp. 261–267.

M. Sichel
Associate Editor